Pozzolanic Activity of Corn Straw Leaf Ash Produced at Different Temperatures and Treated with Portlandite Solution

Tingye Qi,[a,b] Guorui Feng,[a,b,*] and Haochen Wang [a,b]

The effect of calcination temperature on the pozzolanic activity of corn straw leaf ash (CSLA) was evaluated. The CSLA samples calcined at temperatures of 500, 700, and 850 °C were mixed in a portlandite solution for 6 h, and residual samples were obtained. The CSLA and residual samples were analyzed using Fourier transform infrared spectroscopy, X-ray powder diffraction, scanning electron microscopy, X-ray photoelectron spectroscopy, and a contact angle goniometer to determine the vibration bonds, minerals, phase composition, microstructure, Si 2p transformation behavior, and wetting behavior. The conductivity and loss of conductivity with mixing time of the CSLA-portlandite mixed solution was determined. The loss of conductivity of the CSLA prepared at 500 °C was high compared to that of the other calcination temperatures at the same mixing time, which was attributed to the higher amorphous SiO_2 content in the CSLA at 500 °C. Calcium silicate hydrate was easily identified in the CSLA residual samples, and some dense small cubic and nearly spherical shaped calcium silicate hydrate particles were found in the CSLA residual samples at 500 °C. Based on the findings, it is recommended that CSLA be calcined at 500 °C using the cement system in view of higher pozzolanic activity but avoiding excessive agglomeration.

Keywords: Calcination temperature; Pozzolanic activity; Corn straw leaf ash; Portlandite solution

*Contact information: a: College of Mining Technology, Taiyuan University of Technology, Taiyuan 030024, China; b: Shanxi Province Research Center of Green Mining Engineering Technology, Taiyuan 030024, China; *Corresponding author: fgr09000@126.com*

INTRODUCTION

In China, the gross output of corn straw resources is approximately 2.4 billion tons (Vassilev *et al.* 2013; Zhang *et al.* 2016). In recent years, a high amount of corn straw, as a main source of fuel, has been transported to biomass power plants. However, a large amount of the corn straw ash waste needs to be managed with environmentally friendly and economically rational methods. Several studies have focused on the application of corn straw ash. It should be noted that ash with fusion on different components of corn straw possess chemical characteristics that lead to its application in different fields (*e.g.*, fertilizer / adsorbent).

Corn straw is mainly made up of corn cobs, corn straw stems, and corn straw leaves. Corn cob ash is a useful material as a pozzolan for producing blended cement because it contains more than 70% total of SiO_2 and Al_2O_3 (Adesanya and Raheem 2009, 2010). Corn stem ash (CSA) has been mixed with ground blast furnace slag, chrome slag, and pitch in different proportions as a coating material to increase adherence (Binici and Aksogan 2011). In addition, CSA was found to contain amorphous silica, which mixes in aqueous solution, and could be regarded as a potential pozzolanic material (Feng *et al.* 2020).

However, little has been reported on the application of CSLA. Whether or not CSLA has pozzolanic character should be investigated. Some kinds of biomass ash (BA) from agro-industrial by-products have long been known to possess pozzolanic activity, due to having large amounts of silica in amorphous form, which could be used in concrete or as a supplementary cementitious material (Morales *et al.* 2009; Shen *et al.* 2011; Frias *et al.* 2012). Rice husk ash (RHA), palm oil clinker powder, and wheat straw ash have been added in cement-based materials to improve the strength due to the dominant amorphous silica content in their BA, which is useful in pozzolanic materials that react with calcium hydroxide (CH) to produce calcium silicate hydrate (Soares *et al.* 2015).

There are many methods used to investigate the pozzolanic activity of BA (Villar Cociña *et al.* 2018). In general, BA is usually mixed in a saturated portlandite solution to assess the pozzolanic reactivity by measuring the electrical conductivity and testing other chemical properties.

Moraes *et al.* (2016) evaluated the electrical conductivity of CH and pozzolan suspensions to assess the pozzolanic reactivity of sugar cane straw ash and found that sugar cane straw ash is a good pozzolanic material. Van *et al.* (2014) found that the rate of decrease of the electrical conductivity was a suitable parameter for comparing the pozzolanic reactivity of silica fume and RHA. Impedance spectroscopy was used to characterize the pozzolanic activity of RHA. The method is based on the rate of the normalized conductivity change of the $Ca(OH)_2$ and RHA paste during the first 24 h of hydration (Wansom *et al.* 2010). Vichan and Rachan (2013) blended calcium carbide residue with BA and mixed them in water. The $Ca(OH)_2$ reacted with amorphous SiO_2 from BA to produce pozzolanic products.

Table 1. Comparison of Pozzolanic Activity of Different Biomass Ash

Biomass Ash Type	Calcination Temperature	Optimum Calcination Temperature	SiO_2 Percentage Content	Test Method	
Bamboo leaf ash (Villar Cociña *et al.* 2018)	500-700 °C	500 °C	71.77%-74.7%	Mixed with saturated $Ca(OH)_2$ solution	Reduction in conductivity
					SEM observation
					Loss of conductivity
Rice husk ash (Xu *et al.* 2012)	500-800 °C	600 °C	91.71%	X-ray diffraction analysis	
				Compressive strength of mortar	
Sugar cane waste ash (Morales *et al.* 2009)	800, 1000 °C	---	58.61%-70.99%	Mixed with saturated $Ca(OH)_2$ solution	Fixed lime content
					Loss of lime concentration

Moreover, the flocculation or agglomeration properties are important for the mixing of BA in water (Wang *et al.* 2019). A high-quality fluidity of cemented-based slurry is required if the slurry is to be transported long distances through pipelines. If the raw materials show flocculation or agglomeration, then there is an increased blocking risk for transport through pipelines. Flocculation is related to the wetting behavior of the BA. A measurement of the contact angle was performed to reflect the wetting behavior of the BA. The interactions between the surface energies of the BA and water could explain the wetting behavior. If the mixed BA-water colloid was a thermodynamically unstable system with high surface free energy, it would be inclined to reduce the surface areas (wetting behavior) to reduce the surface energy. As a result, BA particles are likely to absorb other BA particles and reduce the surface free energy, which results in excessive agglomeration (Yang *et al.* 2019).

In this study, the pozzolanic properties of CSLA at calcined temperatures of 500, 700, and 850 ℃ were investigated. The electrical conductivities and loss of conductivity (LC) mixing the CSLA samples in CH suspensions for 0 to 6 h were measured. The Si^{4+} concentrations of CSLA mixing in KOH/NaOH solution were evaluated. The mineralogy, microstructure, wetting behavior, and shift of the Si 2p and Al 2p chemical bonds of the CSLA samples before and after mixing in the CH suspensions were investigated. These conclusions are useful to understand the pozzolanic activity behavior of CSLA at different calcination temperatures.

EXPERIMENTAL

Materials

Corn stalk leaves (CSL) were collected from Taiyuan city, Shanxi province, China. The CSL samples were washed with deionized water to remove dust and dried at 20 °C for 7 d. The dried samples were crushed to approximately 1 cm grain size to be able to fully combust them. The samples were calcined in a muffle furnace for 3 h at 500 (CSLA-500), 700 (CSLA-700), and 850 °C (CSLA-850).

Table 2. Chemical Composition of CSL Calcined at 500, 700, and 850 °C

	CSLA-500	CSLA-700	CSLA-850
SiO_2 (wt%)	67.02	72.86	73.53
Al_2O_3 (wt%)	2.15	2.09	2.64
Fe_2O_3 (wt%)	1.01	1.02	1.27
CaO (wt%)	6.78	7.72	7.99
MgO (wt%)	3.68	4.29	4.29
SO_3 (wt%)	2.42	1.96	2.25
TiO_2 (wt%)	0.13	0.12	0.16
K_2O (wt%)	5.24	4.91	3.80
Na_2O (wt%)	0.40	0.50	0.57
P_2O_5 (wt%)	0.94	0.97	1.08
Cl (wt%)	0.39	0.25	—
CuO (wt%)	0.23	0.21	0.10
Loss on Ignition (wt%)	89.41	90.67	91.48
Specific Surface Area (m^2/g)	0.534	0.550	0.633

According to previous research on the chemical compositions of CSLA-500, CSLA-700, and CSLA-850 (Feng *et al.* 2019), the chemical composition and physical characteristics of CSLA depend on the combustion temperature (Table 2). High proportions of SiO_2, CaO, MgO, and K_2O compounds were observed in the CSLA samples. The percentages of main pozzolanic composition (SiO_2 + Al_2O_3 + Fe_3O_4) of CSLA-500, CSLA-700, and CSLA-850 were 70.18, 75.97, and 77.44 wt%, respectively.

The portlandite solution used in this study was a saturated $Ca(OH)_2$ solution, which is prepared by dissolving a sufficient amount of calcium hydroxide powder with a minimum purity of 95% in pure water. Also, the powder was dissolved with the aid of magnetic stirring technology to promote the dissolution, and the stirring rate was 500 rev/min and the stirring time was 20 min.

Methods

Cooled CSLA samples were milled and sieved using a 0.074-mm membrane filter (Huafeng Hardware Instrument Co., Ltd., Shaoxing city, Zhejiang province, China) to maintain the particle size uniformity, and then characterized using a contact angle goniometer (DataPhysics Instruments GmbH, Filderstadt, Germany), Fourier transform infrared spectroscopy (FTIR), X-ray powder diffraction (XRD), X-ray photoelectron spectroscopy (XPS), and scanning electron microscopy (SEM).

The pozzolanic activity of CSLA was determined by evaluating the Si^{4+} concentration from CSLA mixed with 0.1 M and 0.5 M NaOH and KOH solution, respectively, at a liquid-to-solid (L/S) ratio of 0.13 L/g. The CSLA-NaOH (KOH) mixtures were mixed using a magnetic stirring apparatus and kept in a circulated oven at 20 °C for 3 d. The mixed suspensions were filtered using qualitative filter paper, and Si^{4+} concentration in the filter liquor were measured by inductively coupled plasma optical emission spectrometer (ICP-OES, Optima 8300 DV radical; Perkin-Elmer Inc., Waltham, MA, USA) to evaluate the pozzolanic activity of CSLA samples with different calcination temperatures.

The CSLA samples were mixed in a saturated $Ca(OH)_2$ solution at a liquid-to-solid ratio of 0.13 L/g using a magnetic stirring apparatus that stirred the mix for 360 min at 500 rev/min. Simultaneously, the conductivity of the solution was checked at intervals of 1 min over the 6 h mixing time.

After mixing for 6 h, the mixed suspension was filtered, and absolute ethyl alcohol was used to wash the residual samples. The residual samples were dried in an oven at 80 ℃ for 6 h, and the dried CSLA-500 (CSLA-500-CH), CSLA-700 (CSLA-700-CH), and CSLA-850 (CSLA-850-CH) residues were obtained. "CH" here indicates the CSLA residue after mixing with calcium hydroxide (CH) solution. The FTIR, SEM, XRD, and XPS analyses were conducted on the dried residues.

The specific surface area of the CSLA samples was determined using a Malvern Laser Mastersizer S 2000 (Malvern Panalytical Ltd., Malvern, UK). The main chemical compositions of the CSLA (in the form of oxides) were measured using X-ray fluorescence (XRF, ZSX Primus II; Rigaku Co., Tokyo, Japan). The XPS analysis was performed using an AXIS UltraDLD instrument (Kratos Analytical Ltd., Manchester, UK) for surface characterization. Photoelectron emissions were excited using a monochromatic Al Kα line with a photon energy of 1486.67 eV. The microstructure analysis of the CSLA was performed using a JEOLJSM-IT200 electron microscope (JEOL Ltd., Tokyo, Japan) at 25 kV. The samples were gold-coated to prevent charging problems. The minerals of all the CSLA samples were characterized by XRD using an Ultima IV Rigaku diffractometer

(Rigaku Co., Tokyo, Japan) with Cu Kα radiation (λ = 1.54178 Å), a generator voltage of 40.0 kV, and a current of 40.0 mA. The 2θ range of 5 to 80° was applied for all the powdered samples in the continuous scan mode at scanning steps of 0.02° and a rate of 10°/min. The conductivity value of the solution was measured using a Leici DDS-307A conductivity meter (INESA Scientific Instrument Co., Ltd., Shanghai, China), and the criterion pH value was adjusted before every test. Fourier transformed infrared spectroscopy was performed using a Bruker Tensor 27 (Bruker Co., Billerica, MA, USA) in a wavenumber range between 400 and 4000 cm^{-1}. The contact angle between water and the CSLA was measured with the sessile drop method by using the contact angle goniometer, an OCA20 measuring system (DataPhysics Instruments GmbH, Filderstadt, Germany). The results presented were averages from three measurements. The amount of dissolved Si ions in the mixed solution was measured by ICP-OES. The intensity *versus* concentration calibration curve was obtained using a series of Si standard solutions that were prepared based on a conventional calibration process of ICP-OES prior to measurements. The lowest value of Si ions concentration in the mixed solution was measured at 2.476 mg/L.

RESULTS AND DISCUSSION

Dissolution of Si Ions

He *et al.* (1995) evaluated the pozzolanic activity of clay minerals by measuring the amount of dissolved Si ions in the KOH and clay mixed solution. In this study, the pozzolanic activity of CSLA samples were evaluated by Si^{4+} concentration of the CSLA and NaOH mixed solution. From Table 3, CSLA-500 showed a higher Si^{4+} concentration dissolving out from the mixed solution than the CSLA-700 and CSLA-850 samples, which showed that the CSLA-500 possessed higher pozzolanic activity than the CSLA-700 and CSLA-850. It was clear that the Si^{4+} concentration of CSLA mixed in 0.2 M KOH (NaOH) solution was higher than the 0.1 M KOH (NaOH) solution. The Si^{4+} concentration of CSLA mixing in the saturated $Ca(OH)_2$ solution was below 2.476 mg/L because the Si^{4+} could react with Ca^{2+} and OH^-, producing calcium silicate hydrate.

Table 3. The Dissolution of Si^{4+} of CSL Calcined at 500, 700, and 850 °C in the Alkaline Solution

Samples	CSLA-500 (mg/L)	CSLA-700 (mg/L)	CSLA-850 (mg/L)
0.1 M NaOH	177.31	13.632	*
0.2 M NaOH	342.92	43.119	*
0.1 M KOH	170.88	10.148	*
0.2 M KOH	350.94	30.267	*
Saturated $Ca(OH)_2$	*	*	*

*: The Si^{4+} concentration was below 2.476 mg/L

Conductivity Characteristic

Figure 1a shows that the electrical conductivity values decreased for the suspensions during the testing period. These reductions indicate that the chemical reaction progressed in the CSLA-CH suspensions. Moraes *et al.* (2016) concluded that the reaction of dissolved Ca^{2+} and OH^- with pozzolan particles occurs to form stable and insoluble products. For the electrical conductivity, the sequence was CSLA-850 > CSLA-700 >

CSLA-500, which could be explained by the presence of more soluble materials in the CSLA-850. The LC (%) is the main parameter for analyzing the degree of the reaction given in Eq. 1,

$$LC\ (\%) = (C_0 - C_t) / C_0 \times 100 \quad (1)$$

where LC is the loss of conductivity (%), C_0 is the initial conductivity (μS/cm), and C_t is the conductivity at a given time t (μS/cm).

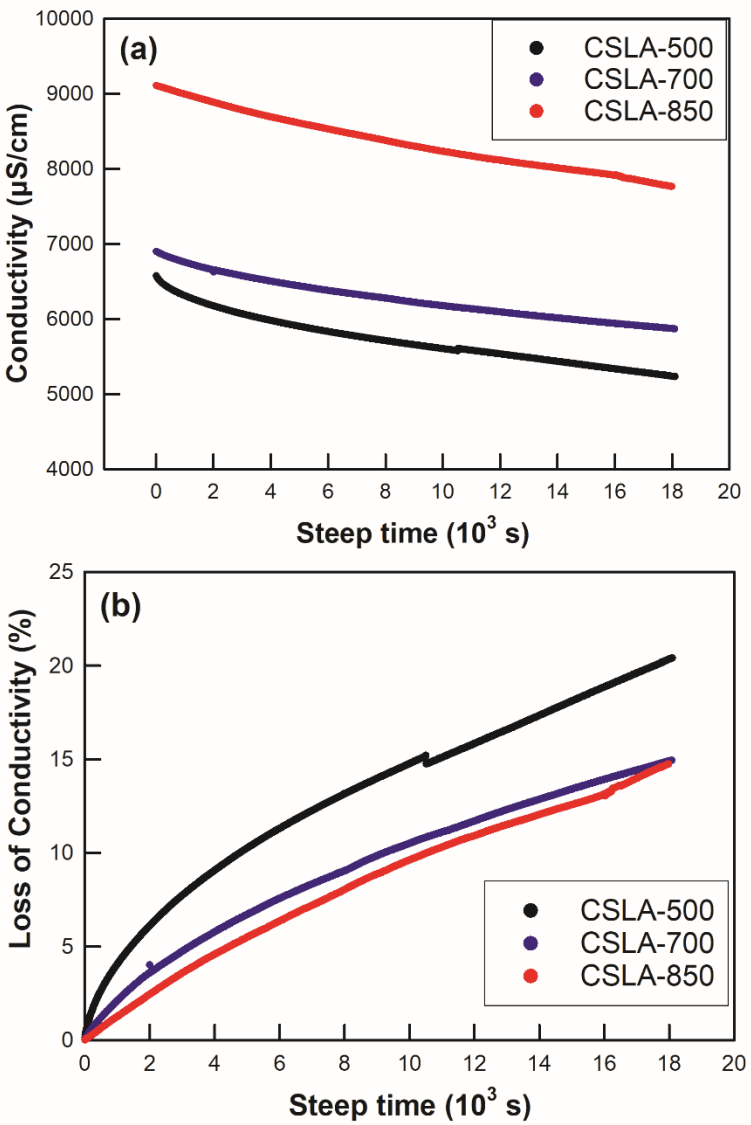

Fig. 1. (a) Relationship between conductivity and steep time; (b) relationship between the loss of conductivity and the steep time for CSLA at different calcination temperatures

From Fig. 1b, the LC (%) value of CSLA-500 was higher than that of the other two samples, which signified that the CSLA-500 had the highest degree of reaction in the CH-suspension. It was found that CSLA-500 had the highest pozzolanic activity and the most amorphous SiO_2 content, the results were the same as the Si^{4+} concentration of the CSLA-500 and NaOH (KOH) mixed solution.

Wetting Behavior

To investigate the surface properties of CSLA with different calcination temperatures, close contact angles were studied to illustrate the similar wetting behaviors of the CSLA microsphere in water. In Fig. 2 the contact angles between the CSLA microsphere particles and the water probes are shown.

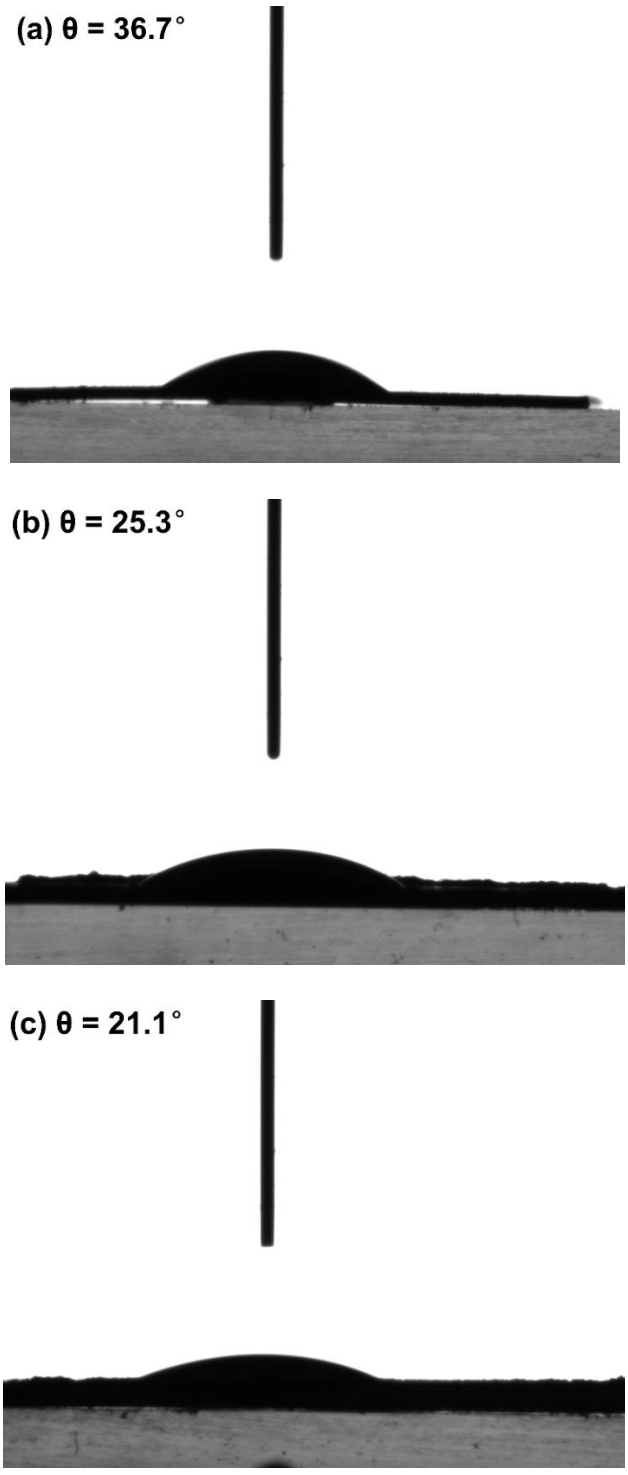

Fig. 2. Contact angles between particles ((a) CSLA-500; (b) CSLA-700; (c) CSLA-850) and water probes

The contact angle of CSLA-500 was much greater than that of the CSLA-700 and CSLA-850 microspheres, indicating less hydrophilic behavior from the CSLA-500 particles. The wetting behavior of CSLA particles is related to the surface free energy or roughness, which can be explained by the excessive agglomeration of CSLA in water. The surface roughness affects the adsorption of water on the particle surface, hence the indirect correlation between agglomeration and contact angle.

When the CSLA was mixed with water, the liquid-vapor and solid-vapor interfaces decreased, and a new solid-liquid interface was created. The contact angle described the equilibrium state with the lowest possible total interfacial energy after wetting. It is described by the combination of Young's and Wenzel's equations, as given in Eq. 2,

$$-\Delta G = \sigma_{LV}[1 + (\cos\theta)/r] \quad (2)$$

where $-\Delta G$ is the change of the surface free energy (J/m^2), σ_{LV} is the surface free energy of the liquid-vapor interface (J/m^2), θ is the contact angle (°), and r is the "roughness factor" defined in Wenzel's equation (Wenzel 1936, 1949) as the ratio of the actual surface area to the area of a smooth surface of the same geometric shape and size.

As shown by Eq. 2, a greater contact angle or smaller roughness factor results in a smaller $-\Delta G$. Hence, the $-\Delta G$ of the wetting procedure of CSLA-500-water was much smaller than that of CSLA-700-water and CSLA-850-water. It is proposed that, as a result, a CSLA-500 particle tended to more easily absorb other CSLA-500 particles to reduce the surface free energy or roughness, which resulted in excessive agglomeration (Wang *et al.* 2019).

The contact angles of the CSLA decreased as the calcination temperature increased. Three factors could explain for this high wettability of the CSLA particles with the increasing calcination temperature in water: 1) The amount of organic ingredient containing nonpolar bonds decreased, and the soluble ionic crystals increased; 2) quartz interacted strongly with water molecules on its surface due to its highly hydrophilic property (Zdziennicka and Janczuk 2011), thus the content of SiO_2 increased, leading to an increase in the wetting ability; 3) the particles with lower surface roughness values have higher hydrophobicities (Ulusoy *et al.* 2003). The CSLA-850 was observed to consist of fine particles with irregular shapes or rough surfaces based on the specific surface area results and SEM observations, which implied the good wettability of these fine particles (Li *et al.* 2011).

Microstructure

As shown in Fig. 3a, some large unburnt ash residues remained in the CSLA-500 samples because of inadequate conversion in the calcination process at 500 °C. The size of the particles ranged from 1 to 10 μm. The morphology was similar to that of RHA with inadequate conversion in the gasification process, and these particles were mainly composed of carbon as biochar (Yao *et al.* 2016).

Figure 3b shows a crisscrossed slab and porous structure in the middle of the CSLA-700 particles. As shown, some crystalline- and polygonal-shaped structures were present in CSLA-850, which revealed that CSLA-850 had a higher agglomeration tendency than the other two calcination temperature samples. In addition, the adhesion and slight caking of small particles were dispersed at the surface of the structure. Moreover, as shown in Table 2, the specific surface area increased as the calcination temperature increased, which can be attributed to crystalline growth leading to the formation of more broken

smaller particles (seen in Fig. 3) and the removal of carbonyl and phenolic hydroxyl of the biochar, leading to cavity growth as the pyrolysis temperature increased (Bai *et al.* 2017).

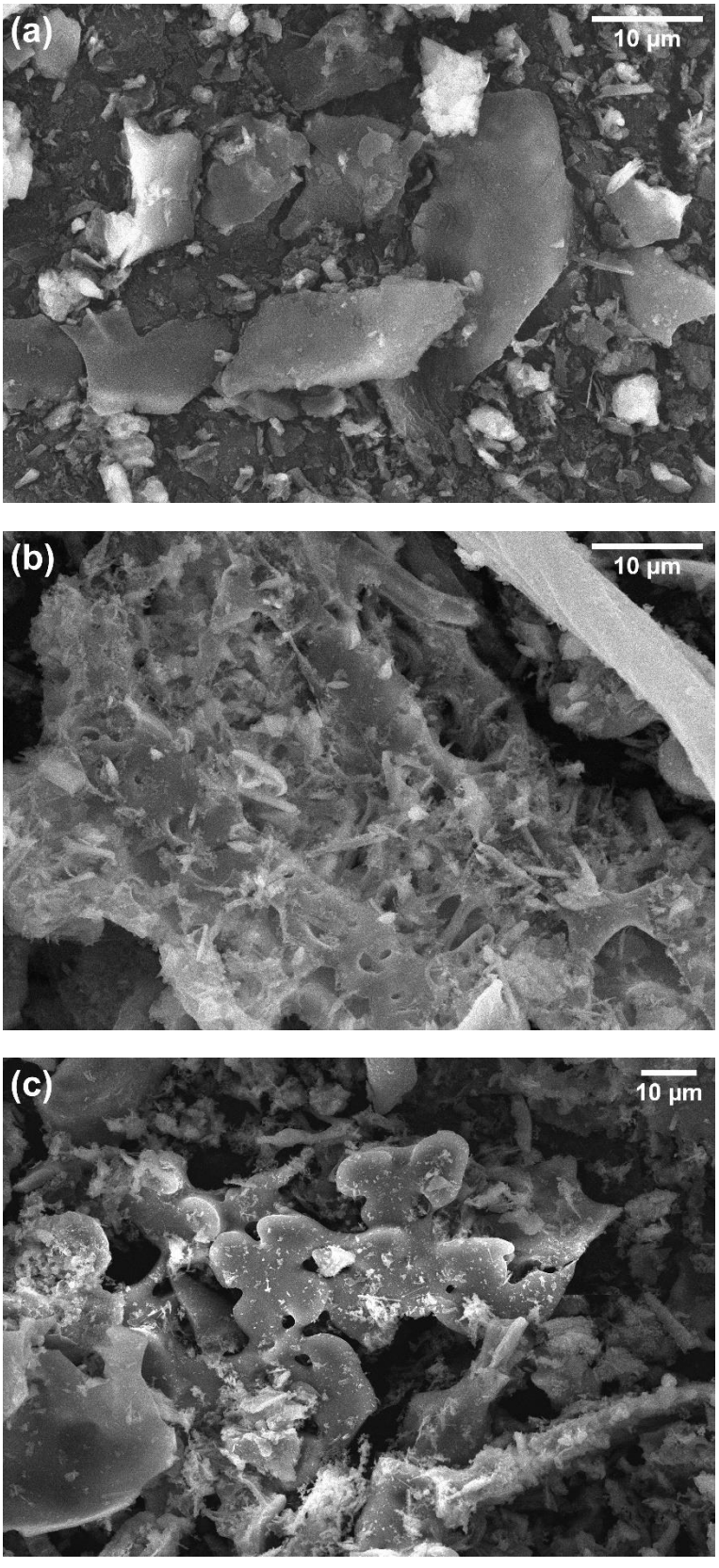

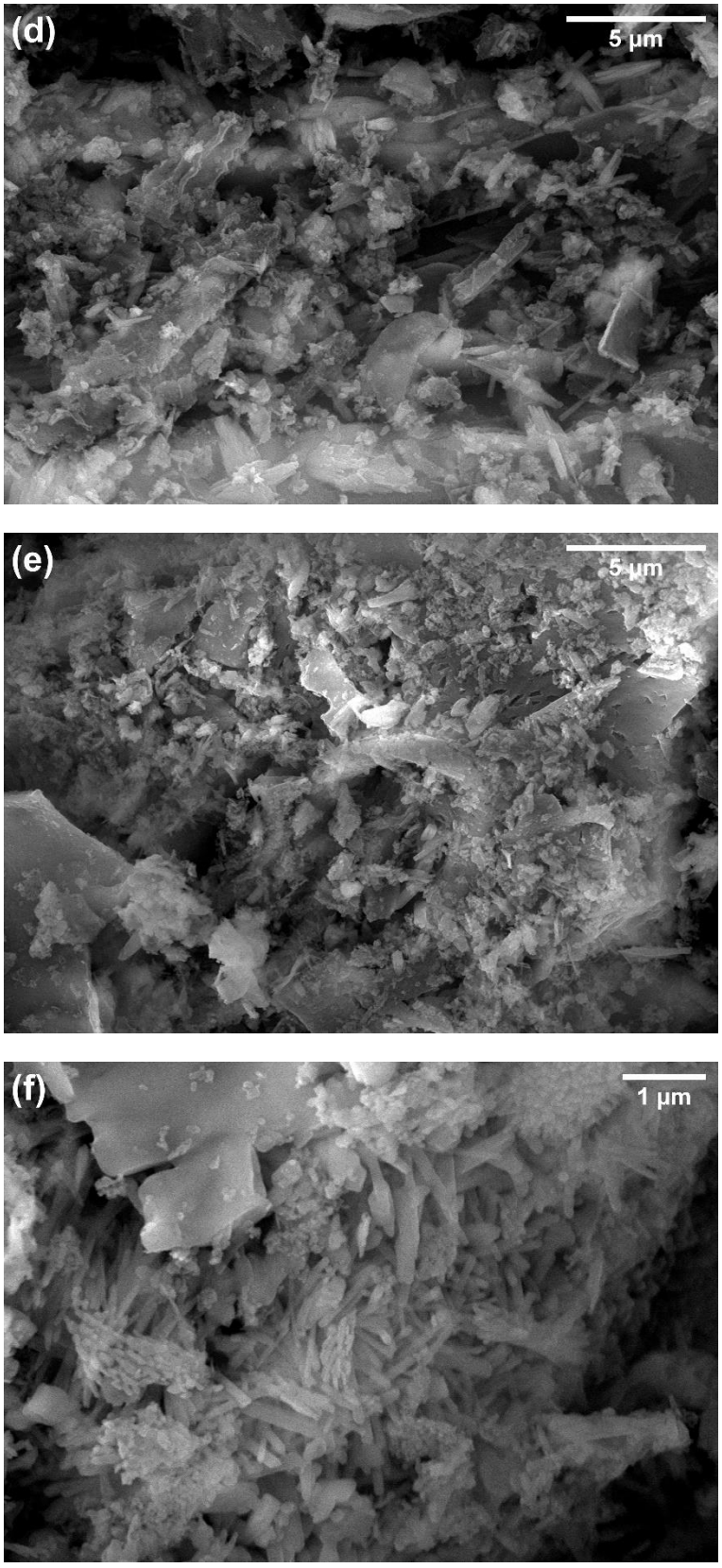

Fig. 3. SEM images of (a) CSLA -500; (b) CSLA-500-CH; (c) CSLA-700; (d) CSLA-700-CH; (e) CSLA-850; (f) CSLA-850-CH

Moreover, a lower specific surface area of CSLA could lead to more pozzolanic reactivity due to the crystalline silica particles having smaller surface area compared with amorphous silica (Van *et al.* 2014; Fernandes *et al.* 2017).

When the CSLA samples were mixed in the CH solution, cubic-like rhombohedral crystals were observed in the CSLA-500-CH and CSLA-700-CH samples (Fig. 3d); these could be $CaCO_3$ particles. The crystallite size of these particles was in the range of 11.55 to 38.1 nm (Altiner 2019). Some small cubic and nearly spherical particles, which could be calcium silicate hydrate, were dispersed at the specimen surface of the CSLA-500-CH and CSLA-700-CH samples (Fig. 3d and 3e). The more compact fibrillar-shaped structure, which could be calcium silicate hydrate, was highlighted on the surface of the CSLA-850-CH particles (Fig. 3f). This phase was rich in Ca, Si, and contains aluminum and iron.

Mineralogy

Table 4 shows the major Al-Si minerals contained in CSLA and the CSLA residues at different calcination temperatures after mixing in CH, as identified from the XRD.

Table 4. Major Si-Al Minerals Contained in the CSLA and CSLA Residuals at Different Calcination Temperatures

Samples	Minerals
CSLA-500	Calcium oxide CaO; Gismondine $CaAl_2Si_2O_8{\cdot}4H_2O$; Anorthite $CaAl_2Si_2O_8$; Aluminum oxide Al_2O_3; Phlogopite $KMg_3(Si_3Al)O_{10}(OH)_2$
CSLA-700	Gismondine $CaAl_2Si_2O_8{\cdot}4H_2O$; Aluminum oxide Al_2O_3 Anorthite $CaAl_2Si_2O_8$; Muscovite $KAl_2(Si_3Al)O_{10}(OH,F)_2$
CSLA-850	Gismondine $CaAl_2Si_2O_8{\cdot}4H_2O$; Aluminum oxide Al_2O_3; Anhydrite $CaSO_4$
CSLA-500-CH	Gismondine $CaAl_2Si_2O_8{\cdot}4H_2O$; Anorthite $CaAl_2Si_2O_8$; Aluminum oxide Al_2O_3; Calcium silicate $CaSi_2O_5$; Calcium silicate hydrate $Ca_2SiO_4{\cdot}xH_2O$; Calcium aluminum oxide $CaAl_{10}O_{18}$
CSLA-700-CH	Gismondine $CaAl_2Si_2O_8{\cdot}4H_2O$; Anorthite $CaAl_2Si_2O_8$; Calcium silicate Ca_2SiO_4; Calcium silicate hydrate $Ca_6Si_3O_{12}{\cdot}H_2O$; Calcium aluminum oxide $Ca_3Al_{10}O_{10}$
CSLA-850-CH	Gismondine $CaAl_2Si_2O_8{\cdot}4H_2O$; Calcium silicate Ca_2SiO_4; Calcium silicate hydrate $Ca_2SiO_4{\cdot}xH_2O$; Aluminum oxide Al_2O_3; Calcium aluminum oxide $Ca_{1.8}Al_2O_{4.8}$

It can be observed from Fig. 4a that SiO_2 was easily identified in CSLA. It should be noted that the other silica polymorphous crystalline form of cristobalite could be found in the CSLA-850 samples. Previous studies showed that the silica phase transformation in RHA begins at 600 and 800 °C, and that the cristobalite phase begins at 800 °C (Kapur 1985; Fernandes *et al.* 2017; Zheng *et al.* 2018). The sylvite was only identified in the CLSA-500 samples. It should be emphasized that the K and Cl contents decreased as the calcination temperature increased, which was related to the condensation mechanisms of KCl vapor during CSL combustion.

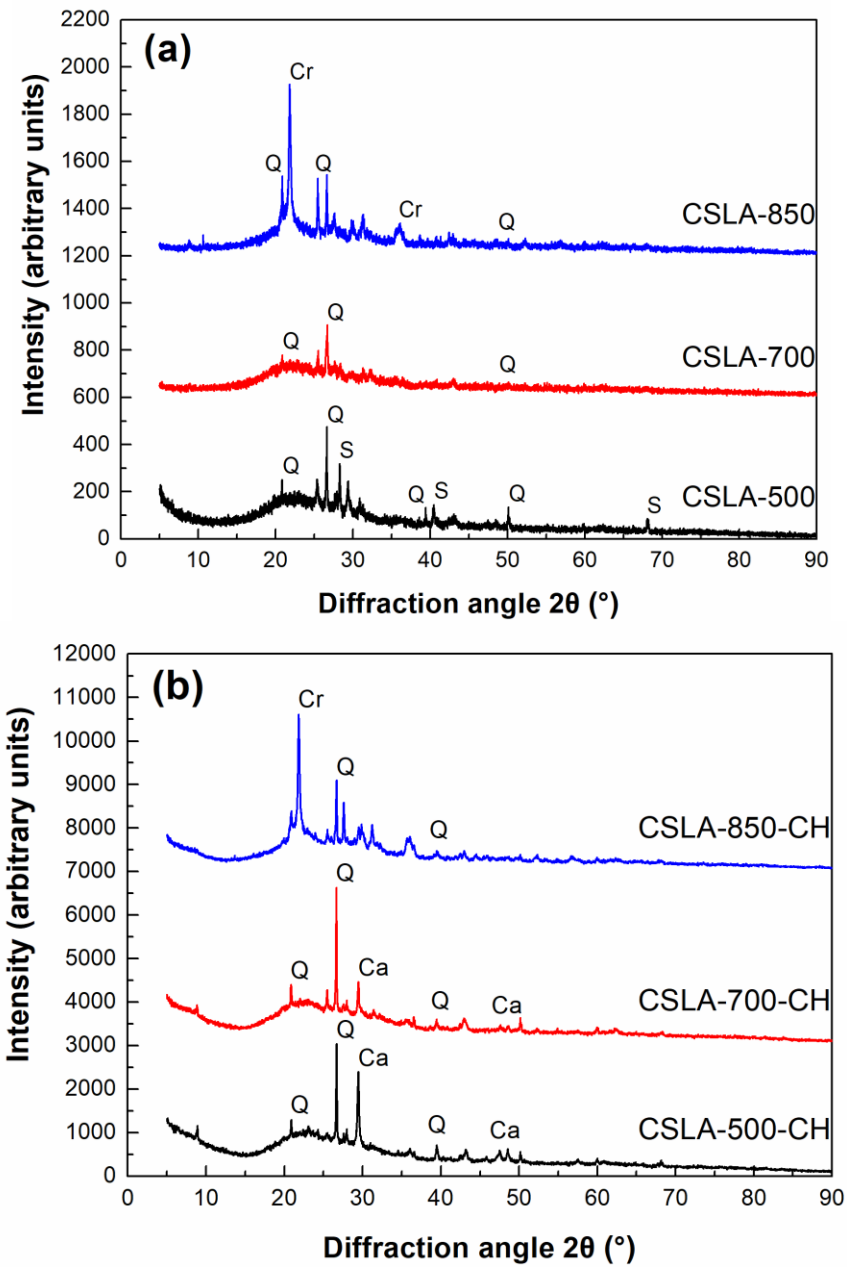

Fig. 4. XRD patterns for (a) CSLA-500, CSLA-700, and CSLA-850; (b) CSLA-500-CH, CSLA-700-CH, and CSLA-850-CH; Key: S = sylvite KCl; Q = quartz SiO_2; Ca = calcite $CaCO_3$; Cr = cristobalite SiO_2

When the CSL was heated at more than 500 °C, K mainly existed as KCl vapor, which could condense on the surface of the CSLA particles during the combustion of CSL. Moreover, KCl either transformed into the gaseous phase or was incorporated into the silicate structure *via* a reaction with Si-containing compounds at more than 500 °C, which can be reflected by the vanish of sylvite in CSLA-700 and CSLA-850 (Nielsen *et al.* 2000; Knudsen *et al.* 2004).

When the CSLA samples were mixed in the CH solution, as shown in Fig. 4b, the soluble minerals, such as lime and sylvite, disappeared in the XRD test. Quartz was identified as a noticeable mineral in the CSLA-CH samples as was calcite, except in the

CSLA-850-CH samples. Gismondine and aluminum oxide were present in all samples. Gismondine was stable in the CH solution. Moreover, as the CSLA was mixed in the CH solution, amorphous aluminum oxide could react with $Ca(OH)_2$ to produce the calcium aluminum oxide, which was found in CSLA-CH samples. In the CSLA-CH samples, calcium silicate hydrate was easily identified in the XRD pattern because the amorphous silica particles in an alkaline solution form silicate precursor (Simonsen *et al.* 2009). The silicate precursors can react with Ca^{2+} to produce calcium silicate hydrate, and the calcium silicate hydrate phase could be observed by SEM in the CSLA residual samples.

Spectral Bands

The bands appeared at approximately 1628 cm^{-1} bending vibrations and at approximately 3435 cm^{-1} stretching vibration, which was related to the presence of water and the presence of O-H groups, respectively (Kataki *et al.* 2017). A narrow band of CSLA-CH near 3435 cm^{-1}, due to O-H stretching, was faintly intensified in the CSLA-CH samples due to the generation of calcium silicate hydrate during mixing in the CH.

Additionally, absorption bands related to the presence of carbonate anions (possible organic matter) were observed at 875 cm^{-1}. These C-O bands disappeared for CSLA-700 and CSLA-850, suggesting that the carbonate that was present in the ash decomposed (decarbonation) at 700 °C and 850 °C or organic matter decomposed. The bands over 1440 to 1480 cm^{-1} are attributed to the presence of a cellulosic derivative and the presence of a C-O stretching bond. A small amount of the C-O stretching bond can attributed to the reaction of $Ca(OH)_2$ with atmospheric CO_2 (Trivedi *et al.* 2018).

The bands appeared at 1108, 1108, and 1096 cm^{-1} of CSLA-500, CSLA-700, and CSLA-850, respectively. As the calcination temperature rose to 850 ℃, the wavenumbers shifted lower, due to the formation of amorphous aluminosilicate bonds caused by the penetration of aluminum ions into the original arrangement of the Si-O-Si skeletal structure (Eiamwijit *et al.* 2015). It should be noted that the 1108, 1108, and 1096 cm^{-1} bands for CSLA-500, CSLA-700, and CSLA-850 shifted to the lower position at 1092, 1088, and 1069 cm^{-1}, respectively, in the wavenumber band after mixing in the CH, which was related to the changed chemical environment around the regularly arranged chain structures of the Si-O bond, together with the formation of Al-O-Si bonds (Tippayasam *et al.* 2016). Moreover, the behavior of shifting to the lower position can be explained by the silica-glassy part from the CSLA particles that react with $Ca(OH)_2$ and form part of the gel due to the band absorption of the silica-glassy that was higher in energy than the one found for gel (Moraes *et al.* 2017). In the low wavenumber region, the bands at 467 and 470 cm^{-1} resulted in the bending vibrations of O-Si-O (Partyka and Lesniak 2016). The bands at approximately 800 cm^{-1} are related to the presence of the tetrahedral bending of Si-O-Al.

The instrument used for XPS was widely applicable for probing the surface chemical composition and atomic structure of BA. Figure 6 shows the shift of the curves of the Si 2p and Al 2p lines obtained for CSLA and CSLA-CH with different calcination temperatures, respectively. According to Kljajević *et al.* (2017) and Zhu *et al.* (2018), the Si 2p lines were mainly resolved into four contributions. The first contribution was pure siloxo Si-O-Si bonds, and the position of Si 2p3/2 was as high as 103.8 eV (Paparazzo *et al.* 1992). The second contribution of the Si 2p3/2 line was situated at approximately 103.1 eV, corresponding to quartz. The third contribution at approximately 103.6 eV was attributed to amorphous silica (Zhu *et al.* 2018), and the fourth contribution was related to Si-OH bonds and was as high as 102.6 eV (Kljajević *et al.* 2017).

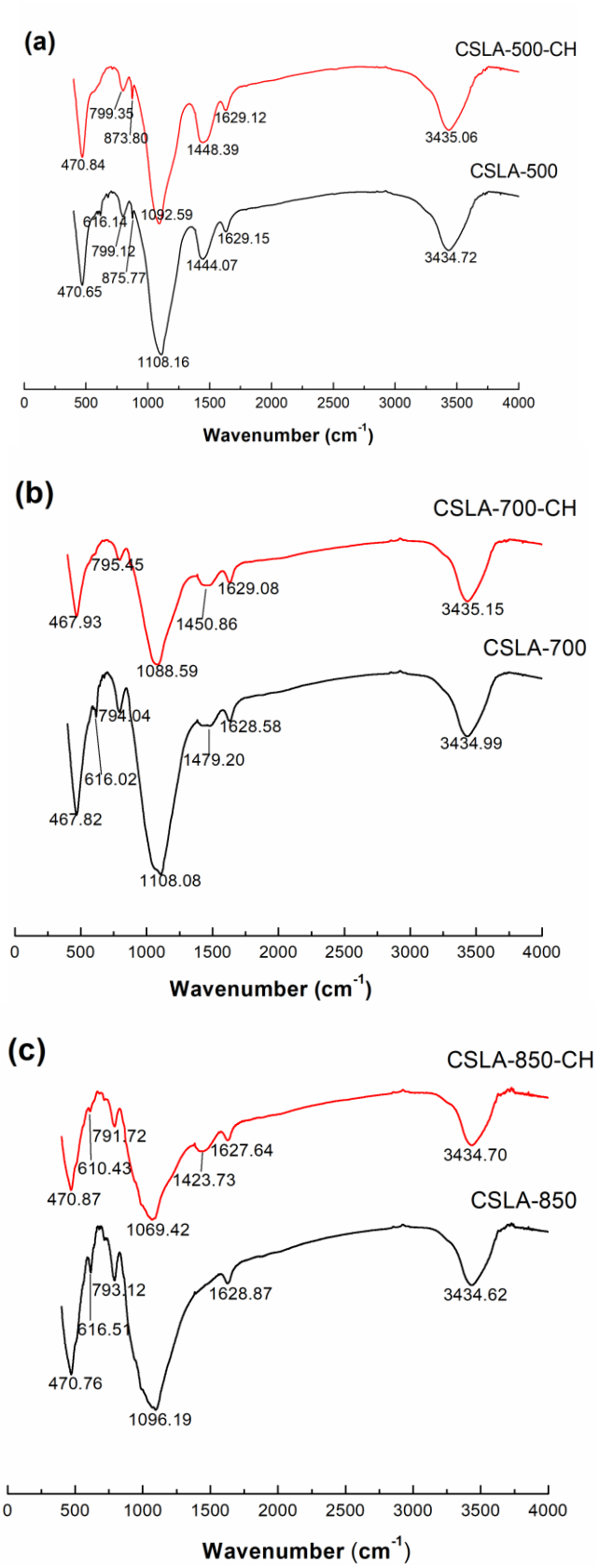

Fig. 5. FTIR spectra of (a) CSLA-500 and CSLA-500-CH; (b) CSLA-700 and CSLA-700-CH; (c) CSLA-850 and CSLA-850-CH

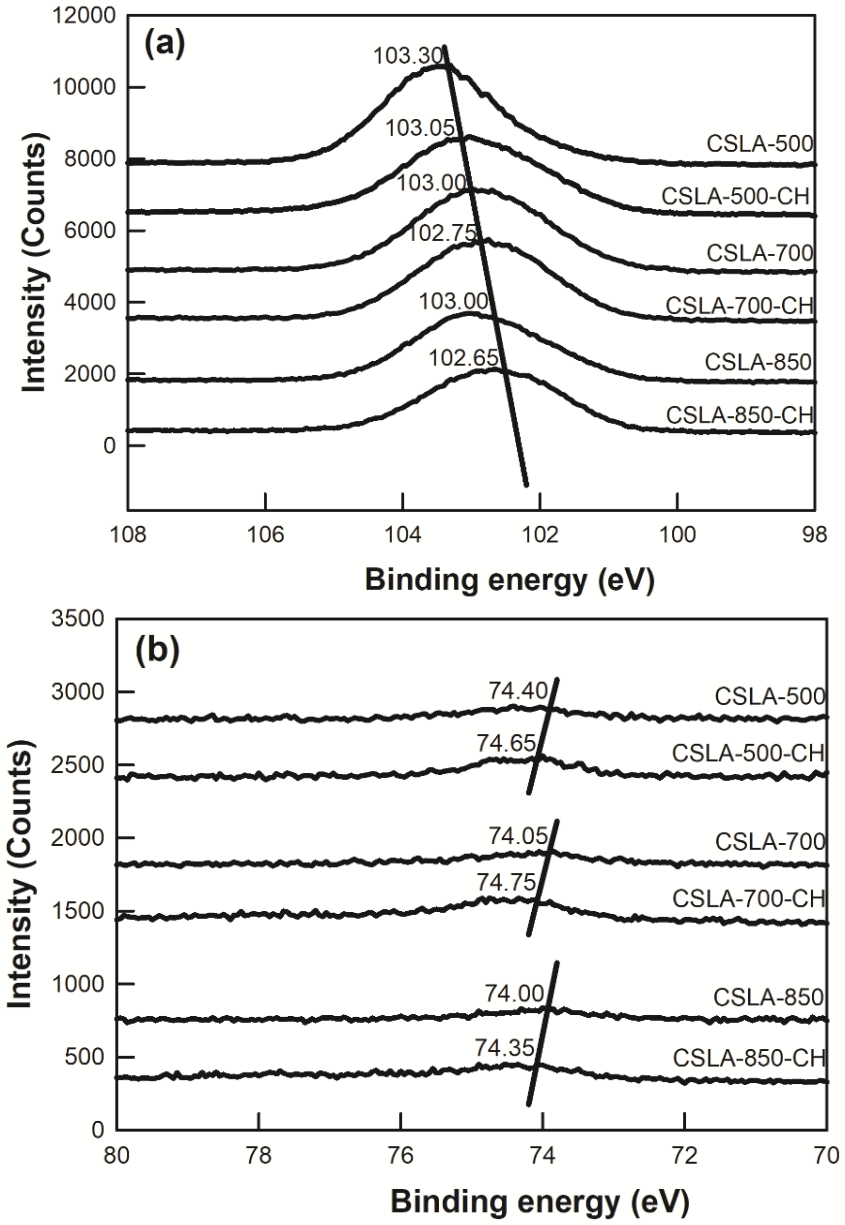

Fig. 6. (a) Si 2p; (b) Al 2p lines shift of the CSLA with calcination temperatures of 500, 700, and 850 °C after mixing in CH solution for 120 min

As the calcination temperature was increased to 700 ℃, the binding energies of Si 2p shifted to a lower position compared to those of CSLA-500 (~ 0.3 eV) (Fig. 6a). It can be concluded that annealing at 700 ℃ resulted in the destruction of some Si-O-Si groups and the formation of another silicon compound. The other possible reason was that some amorphous silica transformed to crystalline silica as calcination temperatures increased.

When the CSLA was mixed in the aqueous solution, the binding energies of Si 2p shifted to a lower position (Fig. 6a). The formation of calcium silicate hydrate by amorphous SiO_2 reacted with $Ca(OH)_2$, which increased the content of the Si-OH bands, leading to the lower position.

The structure of the Al ion is mainly composed of an octahedral-coordinated Al ion and a tetrahedral-coordinated Al ion. The octahedral-coordinated Al ion was more polarizable than the tetrahedral-coordinated Al ion in an electronic environment (Li *et al.* 2008). The Al 2p binding energy of the octahedral-coordinated Al ion was higher than the binding energy of the tetrahedral-coordinated Al ion (Black *et al.* 2003). As shown in Fig. 6b, the peak position of Al 2p3/2 of the CSLA samples shifted to the lower position, indicating that the relative content of Al 2p3/2 for the octahedral-coordinated bond sharply increased as the calcination temperature increased. When the CSLA was mixed in a CH solution, the binding energy of the Al 2p peak remarkably increased (Fig. 6b). This was an Al mineral structural dissimilarity between the CSLA and CSLA residual caused by a change in the electronic and chemical environments. The formation of more calcium aluminum oxide could be responsible for the Al 2p bond transformation behavior.

CONCLUSIONS

1. Silica was the dominant chemical oxide component of corn straw leaf ash (CSLA) samples. The loss of the conductivity sequence followed the order of CSLA-500 > CSLA-700 > CSLA-850 after a particular mixing time, which demonstrated the high pozzolanic activity of CSLA-500 in CH. The Si^{4+} concentration of CSLA-500 when being mixed in the NaOH / KOH solution was higher than the other CSLA samples. The specific surface area of the CSLA samples increased as the calcination temperature increased.
2. KCl was easily identified in the CSLA-500 samples. Crystalline SiO_2 appeared in the CSLA and CSLA-CH samples. Calcium silicate hydrate was identified in the CSLA-CH samples. The SEM results revealed that there were some small cubic and nearly spherical particles present on the surface of CSLA-CH-500, which could be calcium silicate hydrate. The contact angle of CSLA-500 was much greater than that of the CSLA-700 and CSLA-850 microspheres, indicating the less hydrophilic behavior of the CSLA-500 particles.
3. From the Fourier transform infrared (FTIR) results, the amorphous SiO_2 was transformed to calcium silicate hydrate after the CSLA mixed in CH due to the greater intensity of the O-H and Si-O bands shifting to the lower position in the wavenumber. From the XPS results, the Si 2p peak tended to shift to lower binding energies, which may have been due to the formation of more Si-OH of Si 2p after CSLA is mixed in CH. Above all, the CSLA had pozzolanic activity. It is recommended that the optimum calcination temperature of corn stalk leaves used in cement-based systems is 500 °C but it needs to avoid the excessive agglomeration.

ACKNOWLEDGMENTS

This work was supported by the Joint Research Fund under cooperative agreement between NSFC and Funds for Coal-Based Low-Carbon Technology of Shanxi (Nos. U1710258 and U1810120), the National Natural Science Foundation of China (Nos. 51574172 and 51804208), the Key Research and Development Program (Social

Development) of Shanxi Province (201803D31044), and the China Postdoctoral Science Foundation (2018M632423).

REFERENCES CITED

Adesanya, D. A., and Raheem, A. A. (2009). "Development of corn cob ash blended cement," *Constr. Build. Mater.* 23(1), 347-352. DOI: 10.1016/j.conbuildmat.2007.11.013

Adesanya, D. A., and Raheem, A. A. (2010). "A study of the permeability and acid attack of corn cob ash blended cements," *Constr. Build. Mater.* 24(3), 403-409. DOI: 10.1016/j.conbuildmat.2009.02.001

Altiner, M. (2019). "Use of Taguchi approach for synthesis of calcite particles from calcium carbide slag for CO_2 fixation by accelerated mineral carbonation," *Arab. J. Chem.* 12(4), 531-540. DOI: 10.1016/j.arabjc.2018.02.015

Bai, X., Zhou, X., Li, Z., Ni, J., and Bai, X. (2017). "Properties and applications of biochars derived from different biomass feedstock sources," *Int. J. Agric. Biol. Eng.* 10(2) 242-250. DOI: 10.3965/j.ijabe.20171002.2878

Binici, H., and Aksogan, O. (2011). "The use of ground blast furnace slag, chrome slag and corn stem ash mixture as a coating against corrosion," *Constr. Build. Mater.* 25(11), 4197-4201. DOI: 10.1016/j.conbuildmat.2011.04.057

Black, L., Garbev, K., Stemmermann, P., Hallam, K. R., and Allen, G. C. (2003). "Characterisation of crystalline C-S-H phases by X-ray photoelectron spectroscopy," *Cement Concrete Res.* 33(6), 899-911. DOI: 10.1016/s0008-8846(02)01089-x

Eiamwijit, M., Pachana, K., Kaewpirom, S., Rattanasak, U., and Chindaprasirt, P. (2015). "Comparative study on morphology of ground sub-bituminus FBC fly ash geopolymeric material," *Adv. Powder Technol.* 26(4), 1053-1057. DOI: 10.1016/j.apt.2015.04.013

Feng, G., Qi, T., Wang, Z., Bai, J., and Li, Z. (2019). "Physical and chemical characterization of Chinese maize stalk leaf ash: Calcining temperature and aqueous solution," *BioResources* 14(1), 977-995. DOI: 10.15376/biores.14.1.977-995

Feng, G., Qi, T., Xu, G., Zhang, D., Wang, Z., and Li, Z. (2020). "Physical chemical characterization of thermally and aqueous solution treated maize stalk stem ash and its potential use in a cementing system," *Energ. Source. Part A* 42(8), 930-941. DOI: 10.1080/15567036.2019.1602206

Fernandes, I. J., Sanchez, F. A. L., Jurado, J. R., Kieling, A. G., Rocha, T. L. A. C., Moraes, C. A. M., and Sousa, V. C. (2017). "Physical, chemical and electric characterization of thermally treated rice husk ash and its potential application as ceramic raw material," *Adv. Powder Technol.* 28(4), 1228-1236. DOI: 10.1016/j.apt.2017.02.009

Frias, M., Savastano, H., Villar, E., De Rojas, M. I. S., and Santos, S. (2012). "Characterization and properties of blended cement matrices containing activated bamboo leaf wastes," *Cement Concrete Comp.* 34(9), 1019-1023. DOI: 10.1016/j.cemconcomp.2012.05.005

He, C., Osbaeck, B., and Makovicky, E. (1995). "Pozzolanic reactions of six principal clay minerals: Activation, reactivity assessments and technological effects," *Cement Concrete Res.* 25(8), 1691-1702. DOI: 10.1016/0008-8846(95)00165-4

Kapur, P. C. (1985). "Production of reactive bio-silica from the combustion of rice husk in a tube-in-basket (TiB) burner," *Powder Technol.* 44(1), 63-67. DOI: 10.1016/0032-5910(85)85022-1

Kataki, S., Hazarika, S., and Baruah, D. C. (2017). "Investigation on by-products of bioenergy systems (anaerobic digestion and gasification) as potential crop nutrient using FTIR, XRD, SEM analysis and phyto-toxicity test," *J. Environ. Manage.* 196, 201-216. DOI: 10.1016/j.jenvman.2017.02.058

Kljajević, L. M., Nenadović, S. S., Nenadović, M. T., Bundaleski, N. K., Todorović, B. Z., Pavlović, V. B., and Rakocević, Z. L. (2017). "Structural and chemical properties of thermally treated geopolymer samples," *Ceram. Int.* 43(9), 6700-6708. DOI: 10.1016/j.ceramint.2017.02.066

Knudsen, J. N., Jensen, P. A., and Dam-Johansen, K. (2004). "Transformation and release to the gas phase of Cl, K, and S during combustion of annual biomass," *Energ. Fuels* 18(5), 1385-1399. DOI: 10.1021/ef049944q

Li, H., Sun, H., Tie, X., and Xiao, X. (2008). "A new method to evaluate the hydraulic activity of Al-Si materials," *Sci. China Ser. E* 51, 113-120. DOI: 10.1007/s11431-007-0064-7

Li, H., Zhang, J., Zhao, Y., Wu, C., and Zheng, C. (2011). "Wettability of fly ashes from four coal-fired power plants in China," *Ind. Eng. Chem. Res.* 50(13), 7763-7771. DOI: 10.1021/ie2001378

Moraes, J. C. B., Melges, J. L. P., Akasaki, J. L., Tashima, M. M., Soriano, L., Monzo, J., Borrachero, M. V., and Payá, J. (2016). "Pozzolanic reactivity studies on a biomass-derived waste from sugar cane production: Sugar cane straw ash (SCSA)," *ACS Sustain. Chem. Eng.* 4(8), 4273-4279. DOI: 10.1021/acssuschemeng.6b00770

Moraes, J. C. B., Tashima, M. M., Akasaki, J. L., Melges, J. L. P., Monzó, J., Borrachero, M. V., Soriano, L., and Payá, J. (2017). "Effect of sugar cane straw ash (SCSA) as solid precursor and the alkaline activator composition on alkali-activated binders based on blast furnace slag (BFS)," *Constr. Build. Mater.* 144, 214-224. DOI: 10.1016/j.conbuildmat.2017.03.166

Morales, E. V., Villar-Cociña, E., Frías, M., Santos, S. F., and Savastano, Jr., H. (2009). "Effects of calcining conditions on the microstructure of sugar cane waste ashes (SCWA): Influence in the pozzolanic activation," *Cement Concrete Comp.* 31(1), 22-28. DOI: 10.1016/j.cemconcomp.2008.10.004

Nielsen, H. P., Frandsen, F. J., Dam-Johansen, K., and Baxter, L. L. (2000). "The implications of chlorine-associated corrosion on the operation of biomass-fired boilers," *Prog. Energ. Combust.* 26(3), 283-298. DOI: 10.1016/s0360-1285(00)00003-4

Paparazzo, E., Fanfoni, M., Severini, E., and Priori, S. (1992). "Evidence of Si-OH species at the surface of aged silica," *J. Vac. Sci. Technol. A* 10, 2892-2896. DOI: 10.1116/1.577726

Partyka, J., and Lesniak, M. (2016). "Raman and infrared spectroscopy study on structure and microstructure of glass-ceramic materials from SiO_2-Al_2O_3-Na_2O-K_2O-CaO system modified by variable molar ratio of SiO_2/Al_2O_3," *Spectrochim. Acta A* 152, 82-91. DOI: 10.1016/j.saa.2015.07.045

Shen, J., Liu, X., Zhu, S., Zhang, H., and Tan, J. (2011). "Effects of calcination parameters on the silica phase of original and leached rice husk ash," *Mater. Lett.* 65(8), 1179-1183. DOI: 10.1016/j.matlet.2011.01.034

Simonsen, M. E., Sønderby, C., and Søgaard, E. G. (2009). "Synthesis and characterization of silicate polymers," *J. Sol-Gel Sci. Techn.* 50, 372-382. DOI: 10.1007/s10971-009-1907-4

Soares, L. W. O., Braga, R. M., Freitas, J. C. O., Ventura, R. A., Pereira, D. S. S., and Melo, D. M. A. (2015). "The effect of rice husk ash as pozzolan in addition to cement Portland class G for oil well cementing," *J. Petrol. Sci. Eng.* 131, 80-85. DOI: 10.1016/j.petrol.2015.04.009

Tippayasam, C., Balyore, P., Thavorniti, P., Kamseu, E., Leonelli, C., Chindaprasirt, P., and Chaysuwan, D. (2016). "Potassium alkali concentration and heat treatment affected metakaolin-based geopolymer," *Constr. Build. Mater.* 104, 293-297. DOI: 10.1016/j.conbuildmat.2015.11.027

Trivedi, N. S., Mandavgane, S. A., and Chaurasia, A. (2018). "Characterization and valorization of biomass char: A comparison with biomass ash," *Environ. Sci. Pollut. R.* 25, 3458-3467. DOI: 10.1007/s11356-017-0689-4

Ulusoy, U., Yekeler, M., and Hiçyılmaz, C. (2003). "Determination of the shape, morphological and wettability properties of quartz and their correlations," *Miner. Eng.* 16(10), 951-964. DOI: 10.1016/j.mineng.2003.07.002

Van, V. T. A., Rößler, C., Bui, D. D., and Ludwig, H. M. (2014). "Pozzolanic reactivity of mesoporous amorphous rice husk ash in portlandite solution," *Constr. Build. Mater.* 59, 111-119. DOI: 10.1016/j.conbuildmat.2014.02.046

Vassilev, S. V., Baxter, D., Andersen, L. K., and Vassileva, C. G. (2013). "An overview of the composition and application of biomass ash. Part 1. Phase-mineral and chemical composition and classification," *Fuel* 105, 40-76. DOI: 10.1016/j.fuel.2012.09.041

Vichan, S., and Rachan, R. (2013). "Chemical stabilization of soft Bangkok clay using the blend of calcium carbide residue and biomass ash," *Soils Found.* 53(2), 272-281. DOI: 10.1016/j.sandf.2013.02.007

Villar Cociña, E., Savastano, H., Rodier, L., Lefran, M., and Frías, M. (2018). "Pozzolanic characterization of Cuban bamboo leaf ash: Calcining temperature and kinetic parameters," *Waste Biomass Valori.* 9, 691-699. DOI: 10.1007/s12649-016-9741-8

Wang, D., Wang, Q., and Huang, Z. (2019). "Investigation on the poor fluidity of electrically conductive cement-graphite paste: Experiment and simulation," *Mater. Design* 169, Article ID 107679. DOI: 10.1016/j.matdes.2019.107679

Wansom, S., Janjaturaphan, S., and Sinthupinyo, S. (2010). "Characterizing pozzolanic activity of rice husk ash by impedance spectroscopy," *Cement Concrete Res.* 40(12), 1714-1722. DOI: 10.1016/j.cemconres.2010.08.013

Wenzel, R. N. (1936). "Resistance of solid surfaces to wetting by water," *Indust. Eng. Chem.* 28(8), 988-994. DOI: 10.1021/ie50320a024

Wenzel, R. N. (1949). "Surface roughness and contact angle," *J. Phys. Colloid Chem.* 53(9), 1466-1467. DOI: 10.1021/j150474a015

Xu, W., Lo, T. Y., and Memon, S. A. (2012). "Microstructure and reactivity of rice husk ash," *Constr. Build. Mater.* 29, 541-547. DOI: 10.1016/j.conbuildmat.2011.11.005

Yang, L., Zhu, Z., Li, D., Yan, X., and Zhang, H. (2019). "Effects of particle size on the flotation behavior of coal fly ash," *Waste Manage.* 85, 490-497. DOI: 10.1016/j.wasman.2019.01.017

Yao, X., Xu, K., and Liang, Y. (2016). "Comparing the thermo-physical properties of rice husk and rice straw as feedstock for thermochemical conversion and characterization

of their waste ashes from combustion," *BioResources* 11(4), 10549-10564. DOI: 10.15376/biores.11.4.10549-10564

Zdziennicka, A., and Jańczuk, B. (2011). "Effect of anionic surfactant and short-chain alcohol mixtures on adsorption at quartz/water and water/air interfaces and the wettability of quartz," *J. Colloid Interf. Sci.* 354, 396-404. DOI: 10.1016/j.jcis.2010.09.063

Zhang, Z., Han, Z., and Sheng, C. (2016). "Feasibility evaluation of biomass fly ashes from power station using as fertilizer," *Transactions of the Chinese Society of Agricultural Engineering* 32(7), 200-205. DOI: 10.11975/j.issn.1002-6819.2016.07.028

Zheng, R., Ren, Z., Gao, H., Zhang, A., and Bian, Z. (2018). "Effects of calcination on silica phase transition in diatomite," *J. Alloy Compd.* 757, 364-371. DOI: 10.1016/j.jallcom.2018.05.010

Zhu, J., Tang, C., Wei, J., Li, Z., Laipan, M., He, H., Liang, X., Tao, Q., and Cai, L. (2018). "Structural effects on dissolution of silica polymorphs in various solutions," *Inorg. Chim. Acta* 471, 57-65. DOI: 10.1016/j.ica.2017.10.003

Article submitted: July 9, 2020; Peer review completed: September 19, 2020; Revised version received and accepted: September 22, 2020; Published: September 25, 2020.
DOI: 10.15376/biores.15.4.8708-8727